

Geologic proxies for Early Mars atmospheric pressure and climate

For submission to the ROSES-2013 Mars Data Analysis Program (NNH13ZDA001N-MDAP)

1. Table of contents	0
2. Scientific/Technical/Management	1
2.2. Goals and Significance of the proposed study	1
2.3. Scientific Background	1
2.3.1. Small ancient craters constrain paleo-atmospheric pressure	2
2.3.2. Fluvial signatures of climate events on Mars: clearer than Earth.	3
2.3.3. Azimuth dependence of runoff production constrains ancient surface energy balance.	4
2.4. Technical Approach and Methodology	6
2.4.1. Overview and data sets to be used	6
2.4.2. <i>Task 1.</i> Analysis of ancient-crater size-frequency distributions to constrain paleoatmospheric pressure	7
2.4.2.1. Measurement of ancient-crater size-frequency distributions	7
2.4.2.2. Monte Carlo model of crater-atmosphere interactions & data-model comparison	7
2.4.3. <i>Task 2.</i> Basin-scale reconstruction of paleohydrology versus stratigraphy/time	8
2.4.3.1. Details of refinement of stratigraphic and chronologic framework for Aeolis Dorsa	9
2.4.3.2. Paleohydraulic constraints from river deposit measurements	10
2.4.3.3. Volumes and timescales and constraints on runoff intensity, intermittency, event number, and event duration	12
2.4.4. <i>Task 3.</i> Analysis of alluvial-fan catchments to constrain Early Mars surface energy balance	13
2.5. Perceived Impact of the Proposed Work	14
2.6. Relevance of the Proposed Work	14
2.7. Plan of Work	15
2.8. Personnel, Qualifications, and Data-Sharing Plan	15
3. References and Citations	16
4. Biographical Sketches	23

2. Scientific/Technical/Management:

2.1 Executive summary. The overarching goal of this proposal is to provide new constraints on climate scenarios for precipitation-fed runoff on Early Mars (>2.0 Gya). We will analyze HiRISE, CTX, MOC and HRSC data, coupled with physical models of crater-atmosphere interaction and runoff production. We will measure (i) the size-frequency distribution of ancient craters at two sites associated with river deposits; (ii) a stratigraphic log of river-deposit dimensions through >300m of fluvial stratigraphy in a 10⁵ km², wind-exhumed sedimentary basin; (iii) the long profiles of source valley networks for large, relatively young alluvial fans in 7 low-latitude craters, and their catchment slopes and orientations. We will thus obtain:- (i) constraints on paleo-atmospheric pressure stratigraphically coordinated with the sedimentary record of climate change; (ii) constraints on paleo-runoff production versus time for a major sedimentary basin; (iii) through the presence or absence of orientation dependence, a determination of whether the relatively recent runoff events that formed large alluvial fans on Mars were regulated by insolation or by regional/global factors. Both individually and jointly, these proxy measurements will narrow the allowed parameter space for physical models of Early Mars climate.

2.2. Goals and Significance of the proposed study.

To achieve our overarching goal, we will address three primary objectives over this 3-year study.

Task	Goal	Premise
1	Measure size-frequency distributions of ancient craters interbedded with river deposits.	Small impactors are screened from the surface by thick atmospheres, so small ancient craters constrain paleo-atmospheric pressure.
2	Measure river-deposit dimensions in Aeolis Dorsa as a function of stratigraphic position.	Changes in river dimensions with stratigraphic position, and fluvial-deposit volumes, constrain runoff production versus time.
3	Quantify azimuth dependence of alluvial fan source channel networks.	Hypothesis that climates supporting late-stage runoff events were only marginally warmer than snow/ice melt threshold is testable through prediction of strong azimuth (insolation) dependence.

The proposed work will enhance the scientific return from the MRO and MGS missions by using data from CTX, MOC and HiRISE to draw quantitative paleoclimate conclusions.

2.3. Scientific Background.

Atmospheric precipitation (rain or snow/ice melt) was the water source for many of the rivers and streams of Early Mars (Malin et al. 2010, Mangold et al. 2004, Irwin et al. 2005). Physical models (environmental scenarios) for runoff production vary widely (e.g., contrast the mechanisms proposed by Haberle et al. 2012, Kite et al. 2013a, Mischna et al., 2013, Toon et al. 2010, Urata & Toon 2013, Wordsworth et al. 2013). **Lack of convergence in our understanding of what allowed rain or snowmelt on Early Mars is not the result of any lack of model sophistication; rather, what is currently in short supply are paleo-environmental proxies (ideally, time series) to constrain the models, and it is this shortage that the proposed work will address.** Environmental scenarios leave distinguishable fingerprints in the geologic record, through the effect of runoff intensity, intermittency, event number, and event duration on sediment transport, and in the effect of paleo-atmospheric pressure on small-crater size-frequency distributions. Many models only permit runoff for certain ranges of environmental boundary conditions (such as atmospheric pressure above a certain value; Pollack et al. 1987), or

only permit runoff for brief intervals (Toon et al. 2010). Therefore, analysis of geologic proxies has the potential to rule out entire classes of models. The geologic proxies that we have selected for analysis are mutually independent, providing maximum constraints. Task 1 constrains a key boundary condition, atmospheric pressure. Task 2 constrains runoff production with time, which is typically a model output. Task 3 tests whether relatively late-stage runoff was dependent on azimuth – a decisive test of climate scenarios for relatively late-stage runoff in which Mars only just briefly and locally exceeded the melting point, as opposed to scenarios in which conditions were more Earth-like (with a thicker atmosphere moderating local surface energy balance).

2.3.1. Small ancient craters constrain paleo-atmospheric pressure:

Planetary atmospheres brake, ablate, and fragment small asteroids and comets, filtering out small hypervelocity surface impacts. A record of Martian atmospheric paleo-pressure is therefore embedded within cratered volumes of ancient sedimentary rocks: the smaller the ancient craters, the thinner the past atmosphere (Vasavada et al. 1993). CTX and HiRISE images of buried-and-then-exhumed crater populations have allowed us to put this idea into action (Kite et al., 2013d, accepted by *Nature Geoscience*). We obtained (Kite et al., 2013d) a best fit of 760 ± 70 mbar (or 1.6 ± 0.2 bar if rimmed circular mesas are excluded) using measurements of the size-frequency distribution of craters interbedded with river deposits (crater $n = 127$, median diameter ~ 70 m, age probably >3.6 Gyr), in combination with our MDAP-funded Monte Carlo model of small primary crater production (Williams et al., 2013) that has been calibrated against the observed flux of new craters on Mars (Daubar et al., 2013). Because survey incompleteness leads to overestimates of median crater size, we currently interpret our best fits as upper limits. **We**

propose to extend this approach to other key sites, and to refine our model, thus strengthening constraints on paleopressure stratigraphically coordinated with the great drying of Mars. Decay of the CO_2 -dominated atmosphere is thought to be a major driver of Mars climate/habitability evolution. In addition to CO_2 's direct greenhouse effect (e.g. Wordsworth et al. 2010), higher paleopressure primes Mars for transient surface liquid water production by impacts, volcanism, or infrequent orbital conditions, by pressure-broadening the absorption lines of other gases, suppressing evaporitic cooling, and delaying post-impact atmospheric cooling (Toon et al. 2010; Kite et al 2013d). Existing geologic proxy data (e.g. Manga et al. 2012) has not led to convergence among estimates of early Mars pressure, which must balance poorly understood fluxes from volcanic degassing, weathering, and escape to space (Manning et al. 2006). **The central hypothesis to be tested in Task 1 is that at the times when**

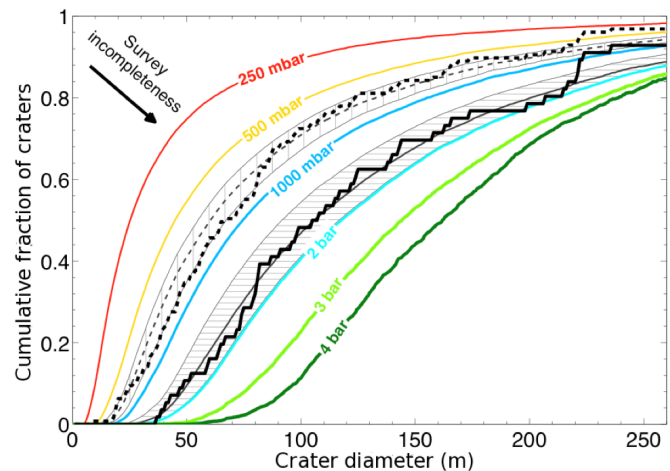


Fig. 1. First data point in our proposed time series of constraints on Mars paleopressure: comparison of model crater size-frequency distributions to observations in Aeolis Dorsa (Kite et al., 2013d). Solid black line: definite embedded craters. Dashed black line: additionally includes rimmed circular mesas. Colored lines: model predictions for atmospheric filtering of small impactors at different pressures. Best fit paleopressure (interpreted as upper limit): thick gray lines. Gray hatched regions show 2σ statistical error for best-fit paleopressure.

large, well-preserved rivers flowed on Mars, the atmospheric pressure was ≤ 1 bar. This hypothesis is motivated by the difficulty of removing a thick atmosphere after the Late Heavy Bombardment (Lammer et al. 2013), modest partitioning of CO₂ into magma at Martian mantle redox conditions (Stanley et al. 2012), and our own preliminary work (Kite et al. 2013d). By constraining paleopressure in the interval when well-preserved rivers flowed, our approach is complementary to isotopic measurements (e.g. Catling 2009) which require massive atmospheric loss predating the stratigraphically-intact geologic record but which do not directly constrain wet-era paleopressure.

2.3.2. Fluvial signatures of climate events on Mars: clearer than Earth.

Climate events in Earth history are recorded in fluvial sediments through changes in fluvial sediment volumes, channel dimensions, and channel-deposit architecture (Foreman et al. 2012, Amundson et al. 2012, Ward et al. 2000). In Task 2, we propose to recover an analogous fluvial record on Mars by measuring paleohydraulic parameters (river-deposit dimensions) versus stratigraphic elevation in Aeolis Dorsa. By so doing we will constrain key unknowns: magnitude, duration, intermittency and number of wet events. Paleodischarge is constrained by channel width and meander wavelength (Burr et al. 2010); minimum runoff duration is found by dividing river-deposit volume by sediment flux (e.g. Jerolmack et al. 2004); intermittency during a wet event is constrained by dividing the duration of runoff by the duration of sediment accumulation (e.g. Kite et al. 2013c); and the number of wet events is greater than or equal to the number of regionally correlatable fluvial packages. Mars has been tectonically quiescent for >3 Ga, making the fluvial record of climate change clearer than on Earth where the strong effects of synfluvial tectonics and base-level change complicate interpretation of the fluvial record in terms of climate

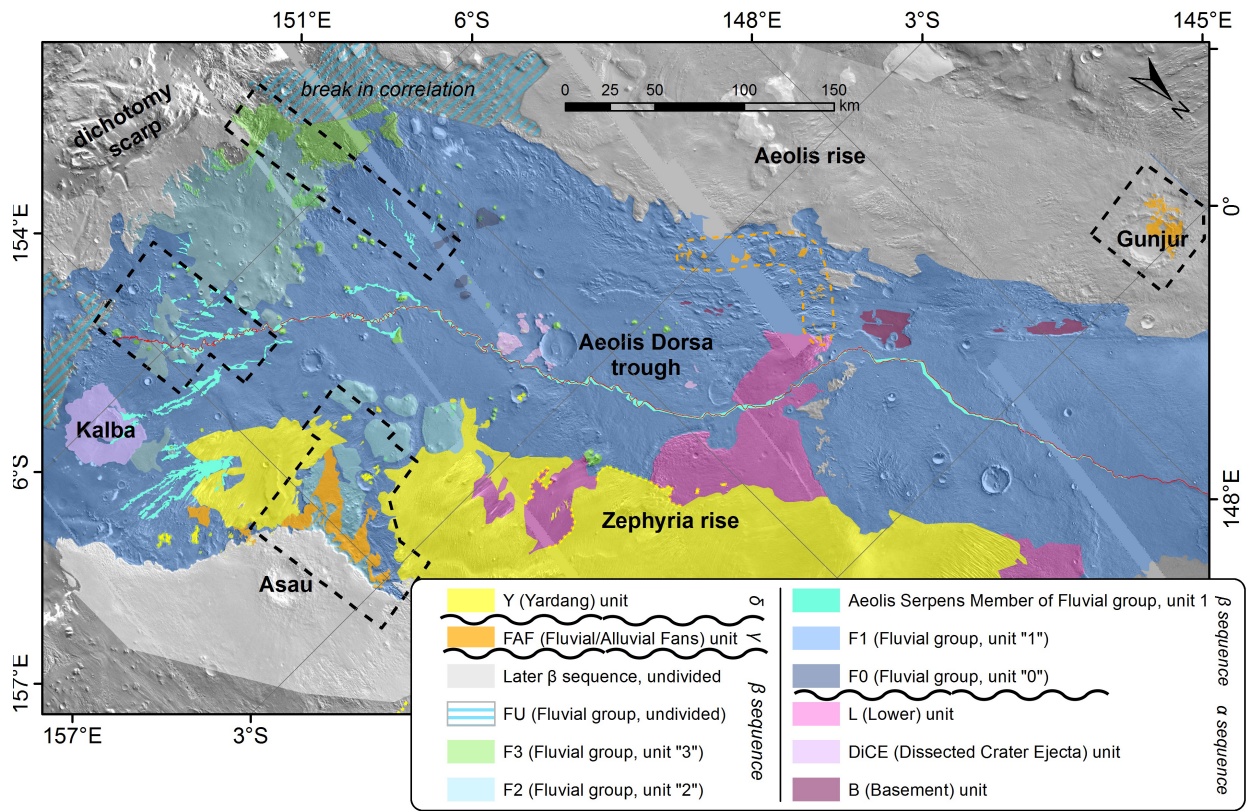


Fig. 2. Simplified geologic unit layer from our preliminary geologic map of Aeolis Dorsa. Contacts picked on a CTX mosaic basemap (not shown). Dashed lines define “transects” (areas to be studied intensively in Task 2). Red line marks course of longest river deposit on Mars.

change (Macklin et al. 2012, Shanley & McCabe 1994). Exceptional preservation of river and stream deposits (and associated unconformities) occurs in Aeolis Dorsa (Howard 2009, Burr et al. 2009, Kite 2012, Lefort et al. 2012; Williams et al. 2013, Kite et al. 2013c).

The river deposits are eroding out of mappable geologic units, which resolve multiple wet events. Initial paleodischarge estimates have been computed using meander wavelength and channel-width scalings (Burr et al. 2010). Crater-counts and stratigraphic analyses (Zimbelman & Scheidt 2012) correlate the meander belts to an interval of ≥ 1 -20 Ma (Kite et al. 2013c) inferred to date to either the central Hesperian or to the Noachian-Hesperian transition (thought to have been a habitability optimum; Howard et al. 2005). The unconformably overlying alluvial fans are much younger (to an extent that we will quantify). Therefore, Aeolis Dorsa contains a time series of information about runoff-sustaining Martian climates. **The overall goal of Task 2 is to condense, as far as possible, the 3D paleohydraulic information in Aeolis Dorsa onto a single dimension - that of stratigraphy - to yield a relative-**

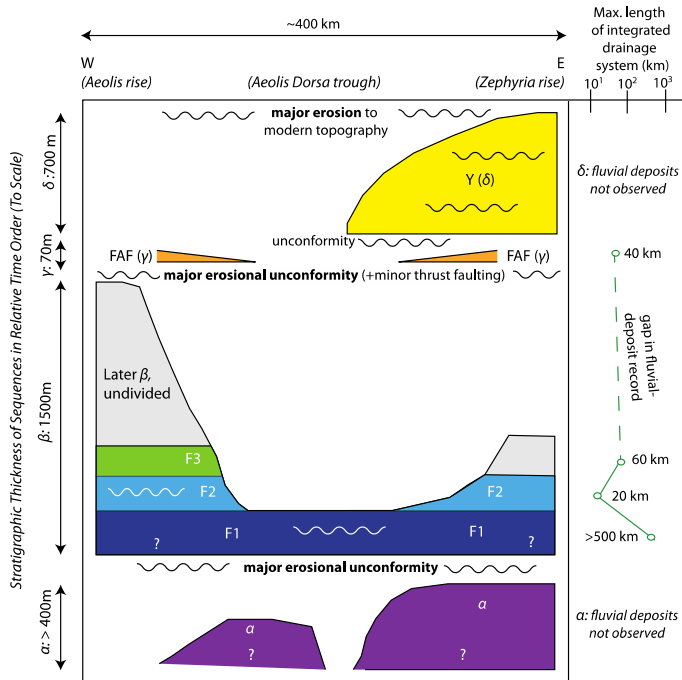


Fig. 3. Preliminary stratigraphic column for Aeolis Dorsa. Preliminary analysis shows stratigraphic trends in the maximum length of integrated drainage system (and in channel widths, not shown).

time series that can be used to constrain models of river-forming climates and climate change on Mars. In preliminary work, we have mapped the major regional erosional unconformities and geologic contacts in Aeolis Dorsa, **establishing an allostratigraphic framework for Task 2** (Fig. 3, Kite et al., 2013e) – all fluvial paleoproxies will be mapped relative to geologic contacts. The proposed stratigraphically-resolved study of multiple generations of river deposits (Fig. 3) can in principle provide a more complete set of constraints than techniques based on river erosion, which constrain the *total* duration of wet conditions as a function of wet-event magnitude (e.g. Hoke et al. 2011), or work constraining the duration of *individual, late-stage* wet events from sedimentary deposits (Armitage et al. 2011).

2.3.3. Insolation (azimuth) dependence of runoff production constrains ancient surface energy balance. The sole sediment and water source for most large alluvial fans on Mars is steep dendritic valley networks incised into the interior crater walls of the alluvial-fan-hosting craters (Morgan et al., in press). Sediment and water pathways from alcoves to fans are simple, short, and direct (Morgan et al., in press). In Task 3, the measurement objective is to map out the convexity and slope of source valley networks for alluvial-fan-bearing craters over a range of azimuths for each crater, and to determine the paleo-insolation on all hillslopes draining into those networks. **Our proposed work complements studies of alluvial fan deposits (i.e. sediment sinks; Williams et al. 2011, Wilson et al. 2013, Morgan et al. in**

press) by measuring the detailed geometry of sediment *source* regions, which have been much less studied. The overall hypothesis to be tested is that the valleys resulted from melting of snow or ice over long timescales under a relatively thin atmosphere (e.g. Grant & Wilson 2012, Kite et al. 2013a). If that was the case, then valley morphometry should depend on valley paleo-insolation, which we will compute for all past orbital parameters using our snowmelt model ISEE-Mars (Kite et al. 2013a).

The physical basis for our hypothesis test is as follows. Insolation (local radiative equilibrium) is overwhelmingly important for surface temperature on today's Mars – turbulent exchange with the 6 mbar atmosphere is secondary. Because (away from the equator) surface orientation strongly affects mean and peak insolation (e.g. Costard et al. 2002), azimuth dependence is ubiquitous in Late Amazonian records of melting and runoff on steep slopes (e.g., Kreslavsky & Head 2003, Balme et al. 2006, Dickson et al. 2007, Conway & Mangold 2013). Insolation dictates both snow/ice stability (water substance availability) and the energy available for melting. On 1-bar Earth, by contrast, atmosphere-surface temperature contrasts are small, elevation controls geomorphology (e.g. Egholm et al. 2009), and insolation effects on geomorphology are subtle (e.g., Petroff et al. 2012). Models indicate a transition at $\sim 1/4$ bar (Forget et al. 2013); at higher pressures, turbulent fluxes between atmosphere and surface dominate surface energy balance. It has been suggested that Late Noachian / Early Hesperian valley networks show elevation control (Scanlon et al. 2013), consistent with loss of atmospheric pressure over time. **We hypothesize that at the relatively late time of large-alluvial-fan formation (Hesperian or Early Amazonian; Grant & Wilson 2011, Mangold et al. 2012), the atmosphere was thin enough for runoff to be aspect dependent.** Our hypothesis is motivated by (i) theory suggesting strong insolation control of liquid water availability (e.g. Kite et al. 2013a), (ii) detailed analysis supporting snowmelt as the water source for alluvial fan formation at Saheki Crater (Morgan et al., in press), (iii) data showing that the orientation distribution of entire alluvial fans has peaks at N and S (Wilson et al. 2013), and (iv) the strong azimuth dependence of late Amazonian fluvial landforms – we propose to determine if this azimuth dependence extends further into the past.

The measurement targets for the hypothesis test are the small valley networks incised into crater rims that form the sediment and water source regions of the large alluvial fans. Long, N-S trending valleys drain E- and W-facing hillslopes. Conversely, long, E-W trending valleys drain N- and S-facing hillslopes. Therefore, for catchments (such as our measurement targets) where the valley walls constitute most or all of the valley catchment, azimuth dependence in runoff production on hillslopes (Morgan et al. 2010) is reflected in azimuth dependence in valley streamflow. In turn, azimuth dependence in valley streamflow will lead to more erosion per unit time for valleys trending at azimuths associated with a higher streamflow, leading to longer valleys, and shallower valley-floor slopes, for a given drainage area. (This is true whether or not the network is close to steady state, and whether erosion is detachment- or transport-limited). **Therefore, the presence/absence of azimuth dependence within alluvial fan source networks is a fundamental geomorphic signature of basic climate parameters.**

Azimuth dependence in runoff production on valley slopes is a robust prediction of environmental scenarios in which Mars only just briefly and locally exceeded the melting point (e.g. Clow 1987). In such scenarios, Mars' atmosphere is relatively thin and direct insolation is the main source of energy for melting. We will utilize a flexible physical model of snow/ice stability and melt (ISEE-Mars; thoroughly described in Kite et al. 2013a) to predict azimuth dependences in detail and compare to data. A metastable warm, wet hydrologic cycle (Baker et

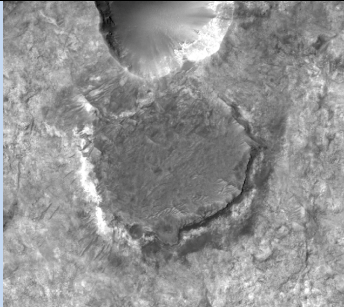
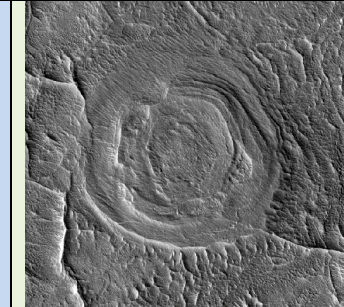
al. 1991, Segura et al. 2012) – in fact any thick-atmosphere climate state (Wordsworth et al. 2013) – would not produce strong orientation dependence. Therefore, the presence or absence of aspect dependence is a straightforward test of Early Mars climate models.

2.4. Technical Approach and Methodology.

2.4.1. Overview and data sets to be used:

We will use CTX, HiRISE, HRSC, MOC and MOLA data (all publicly available on the PDS). For each Task, we will gather MOLA-controlled CTX and/or HiRISE stereo DTMs, to include production of new DTMs in SOCET SET using NGATE (Kirk et al. 2008). A conservative (upper) limit on the total DTM construction lien is 5 HiRISE DTMs (in addition to 5 HiRISE DTMs that we have already constructed for these Tasks) and 15 CTX DTMs (in addition to 2 CTX DTMs that we have already constructed for these Tasks). The PI and Dr. Lucas have extensive experience of stereo DTM construction and we anticipate <1 person-week per DTM. Using the DTMs and orthoimages, as well as mono images in areas bridging the DTMs, the proposal team will manually pick polylines corresponding to geologic features (e.g. crater rims, channel-belt margins, source valley-floors) in ArcGIS 10.1. These polylines will be automatically analyzed using MATLAB to obtain summary data (e.g. crater diameters, meander wavelengths, source valley-floor slopes). Finally, we will convert the measurements into environmental

Table 1: Sites selected for measurement of ancient crater size-frequency distributions.

Site	SE Aeolis Dorsa (Kite et al. 2013d)	Mawrth (proposed)	East Meridiani, SW of Capen (proposed)
Example style of preservation	 <i>Crater (240m across) interbedded with river deposits.</i>	 <i>Crater (~100m across) was infilled by dark capping unit, now forms outlier</i>	 <i>Crater (~160m across) was infilled by layered sediments, now forms outlier</i>
Geologic context	Inverted river channels Layered sedimentary rocks (Kite et al. 2013d)	Phyllosilicates, some sulfates, some inverted channels (Noe Dobrea 2010)	Inverted river channels Layered sedimentary rocks (Hynek & di Achille, in press)
Example stereopair	ESP_019104_1740/ ESP_017548_1740	ESP_026811_2045/ ESP_025123_2045	ESP_021654_1855/ ESP_031212_1855
Published global sedimentary correlations	Intermediate/Younger (Aeolis: Grotzinger & Milliken 2012, Ehlmann et al. 2011).	Oldest (Ehlmann et al. 2011, Grotzinger & Milliken 2012)	Intermediate/Younger (Meridiani: Ehlmann et al. 2011, Grotzinger & Milliken 2012)
Other age estimates	Noachian-Hesperian transition (Kite et al. 2013c).	~ 3.7 Gya (dark capping unit), > 3.9 Gya (main layered unit) (Loizeau et al. 2012)	Early through Late Hesperian (SW of Capen: Hynek & di Achille, in press)
Model used & paleopressure inferred	<i>Old model:</i> $\leq 760 \pm 70$ mbar (Kite et al. 2013d) <i>To Be Determined</i>	<i>Using Improved Model:</i> <i>By The Proposed</i>	<i>Investigation</i>

constraints, in part by comparison with quantitative physical models that we have developed previously (Kite et al. 2013a, Williams et al. 2013) and will refine as part of the proposed work. While the workflow has many common elements, the final environmental parameters to be constrained are selected to be as orthogonal as possible, allowing reduction of the allowed parameter space for Early Mars climate along multiple dimensions.

2.4.2. Task 1. Analysis of ancient-crater size-frequency distributions to constrain paleoatmospheric pressure. In this Task, we will compare size-frequency distributions of embedded craters to a forward model of atmosphere-impactor interactions. We have selected Mawrth and East Meridiani for analysis because they have distinct inferred ages and crater-preservation style from our published SE Aeolis Dorsa site (Table 1), while each also showing a large number of apparent embedded craters in mono images. In support of this workflow, we will additionally carry out geologic context mapping on a CTX base for the purpose of stratigraphic placement of craters and improved age estimates. Based on the best fits and age control, we will derive a time series of paleopressure constraints. Extension to new sites will closely follow the workflow that is thoroughly described in our initial paper (Kite et al. 2013d).

2.4.2.1. Measurement of ancient-crater size-frequency distributions.

The sizes of the study regions are chosen as follows. By resampling the crater population at our preliminary-work site, we have determined that 45 craters are sufficient for a 95% probability that statistical error in median crater diameter is less than half of the sum in quadrature of hard-to-reduce systematic errors in target strength and target density. Based on the embedded-crater density measured in SE Aeolis Dorsa (Kite et al. 2013d), and comparison to HiRISE JP2s for Mawrth and East Meridiani, as little as 1 HiRISE image may be required; we will feed back to additional images / stereopairs if needed. Our approach relies only on crater size-frequency *distributions*, and does not require knowledge of the absolute frequency of impacts (which has changed over time).

Craters are classified as syndepositional, candidate syndepositional, or synerosional, based on a checklist that we have used previously (Table 1 in Kite et al. 2013d). In preliminary work (Kite et al., 2013d) we found that HiRISE resolution was required to classify small craters, and DTMs were also helpful in classification. For Mawrth, embeds are obvious (at least at the stratigraphic level of the dark capping unit, Table 1 in this proposal) so mono images are likely to be sufficient. We conservatively assume DTMs are required for both sites. If it subsequently turns out that site ages are indistinguishable, then multiple sites (differing in style of preservation, target lithology, etc) will allow three tries at the tightest possible constraint on characteristic Early Mars paleopressure.

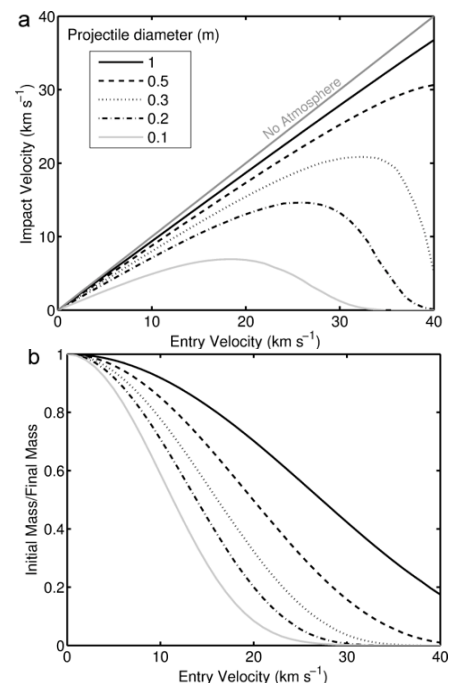


Fig. 4. (from Williams et al. 2013.) (a) Initial velocity versus final velocity, and (b) the ratio of initial and final projectile mass versus initial velocity, for a range of projectile diameters (10 cm – 1 m) where objects have properties of ordinary chondrites. Smaller faster objects are more effectively decelerated and ablated.

2.4.2.2. Monte Carlo model of crater-atmosphere interactions (see Williams et al. 2013 for details of this model). We build a synthetic impactor population by drawing randomly from the size distribution of Brown et al. (2002) and the initial-velocity distribution of Davis (1993). Each population contains 3% irons, 29% chondrites, 33% carbonaceous chondrites, 26% cometary objects, and 9% “soft cometary” objects (following Ceplecha et al. 1998) with densities and ablation coefficients set following Ceplecha et al. 1998. We advect these populations to the surface through the model atmosphere, which drains kinetic energy from impactors via drag and ablation. Fragmentation occurs when ram pressure exceeds 650 kPa, chosen to match the frequency of crater clusters on today’s Mars (Daubar et al. 2013), and within the range reported for Earth fireballs. We do not track secondary craters, because meter-sized endoatmospheric projectiles are likely to be braked to low speeds for the relatively thick atmospheres we are evaluating. In other words, if wet-era small craters are secondaries, then wet-era paleopressure was $\lesssim 1$ bar. Target properties are set based on facies analysis of the target rocks (alluvium in SE Aeolis Dorsa; Kite et al. 2013d). Crater sizes are calculated using π -group scaling (Holsapple et al. 1993). We will refine our model by tracking planet curvature and the changing angle of descent relative to the surface, and use the improved model to recalculate our initial estimates at SE Aeolis Dorsa.

Paleopressure is found by bayesian fitting of the data to cratering-model output. In principle our method can constrain atmospheres as thin as ~ 200 mbar (limited by DTM resolution). For each trial paleopressure P , we run enough randomized cases to build up a smooth crater distribution $\lambda = p(D, P)$, where D is crater diameter. The probability of obtaining the observed number of craters Y in a narrow D bin is given by Poisson statistics:- $p(Y | D, P) = \frac{\bar{\lambda}^Y \exp(-\bar{\lambda})}{Y!}$ (overbar corresponds to scaling for the overall number of impacts observed). The overall likelihood of the data given the model is the sum of the logs of the probabilities over all D bins (Wall & Jenkins 2012). The procedure is thoroughly described in Kite et al. (2013d).

2.4.3. Task 2. Basin-scale reconstruction of paleohydrology versus stratigraphy/time.

Our Task 2 workflow blends traditional geologic mapping (structure contours) with more modern statistical techniques to systematically extract maximum paleohydrologic / stratigraphic information for Aeolis Dorsa from HiRISE and CTX data. We anticipate spending the majority of our FTE effort on Task 2. We will (1) define a quantitative stratigraphic framework (§2.4.3.1); (2) measure paleohydraulic proxy parameters and stratigraphic-architecture parameters, and align them with the stratigraphic framework (§2.4.3.2); and then (3) constrain wet-event parameters through volume and timescale calculations (§2.4.3.3). We have identified 4 key regions within Aeolis Dorsa, which we term “transects” (Fig. 2). Transects are selected based on quality of preservation (high), geographic distribution (spanning the basin with emphasis on the S portion where the density of well-preserved channel deposits is highest), stratigraphic distribution (spanning all fluvial and alluvial units based on our preliminary allostratigraphic framework, Fig. 3), a total area that can be readily measured in the available time based on the rate of measurement established in our preliminary work (Kite et al. 2013cde), and availability in the PDS of CTX stereo coverage (which is complete for all transects). Just as in terrestrial mapping (e.g. Macdonald et al. 2012), our approach will be to document transects in detail (including generation of CTX DTMs over the full area of each transect), and then draw fence diagrams to interpolate between transects.

First (§2.4.3.1), using our CTX base map supplemented by HiRISE, HRSC and MOC images, we will map contacts across Aeolis Dorsa, refining our preliminary map (Fig 2). We will

interpolate all contacts to generate structure contours using kriging, which yields a best estimate and an error. Where stereo DTMs are available, we will assign elevation values from the stereo DTM for all points on contact polylines, and then krige between those points. Where DTMs are not available, we will first linearly interpolate along PEDR tracks crossing the contact to obtain elevation values for the intersections between PEDR tracks and contact polylines, and then krige the contact surfaces using only those intersections. We will generate isopachs from these surfaces (Fig. 5a), reconstruct paleotopography on all unconformity surfaces, and interpret the resulting macrostratigraphy in terms of erosional and depositional processes (Sloss 1963, Howard 2007).

Next, we will (§2.4.3.2) thoroughly document all paleohydraulic proxies (Hajek & Wolinsky 2012) in the transect areas and tag each measurement with a best-estimate relative stratigraphic distance normal to adjacent contact surfaces, as well as an error in this stratigraphic position (adding in quadrature the surface elevation uncertainty due to DTM error, contact-position uncertainty due to kriging error, and contact-orientation uncertainty associated with kriging error). Weighting each paleohydraulic-proxy measurement by the stratigraphic-position uncertainty kernels thus obtained, we will then compute the mean and standard deviation of each paleohydraulic proxy for each geologic unit (considering each transect separately). We will test for the presence or absence of statistically significant differences between geological units, and for linear trends in each paleohydraulic proxy *within* each geologic unit. We will also explore the stratigraphic height dependence (across unit boundaries) of the paleohydraulic proxies using nonparametric fitting methods (Rasmussen & Williams 2006). We hypothesize that runoff trends are regionally coherent across the ~400km-wide basin. We will test this hypothesis by comparing the stratigraphic height dependence of the paleohydraulic proxies between transects. If regional coherence is observed, then we will aggregate all proxy data onto a single stratigraphic column, including measurements falling outside transect areas. If time permits, we will also measure the metrics in the gaps between the transects.

Finally, we will (§2.4.3.3) through volume and timescale calculations, constrain the duration, intermittency, number and magnitude of wet events.

2.4.3.1. Details of refinement of stratigraphic and chronologic framework. An example isopach is shown in Fig. 5a for F2 (Fluvial group, unit “2”). This unit is defined by an abrupt change in orbital facies that appears consistently at ~2300 m, which we interpret as a contact. Above this elevation, F2 is recognized as a slope-former, with smooth erosional expression (lacking yardangs); densely peppered with rimless craters; crater density larger than the units which envelop it; generally darker in tone in CTX than adjacent units, and associated with modern aeolian bedforms (interpretation: sediment source for these bedforms is erosion of F2). Analogous reasoning applies to the other units shown in Fig. 2.

We will use the contact/isopach dataset to test the hypothesis (e.g. Davila et al. 2013) of ancient equatorial ice sheets on Mars. Removal of ice bodies interbedded with fluviodeltaic sediments (Levy et al. 2013) can leave characteristic angular disconformities, lacking for differential compaction (Lefort et al. 2012). Differential compaction of crater-infilling sediments predicts a smooth subsidence pattern with maxima near crater centers (Buczowski et al. 2005); a lumpier pattern is predicted following sublimation of ice, and maximum subsidence can be near the crater rim.

We will count all craters (Fig. 5b) larger than 250m across Aeolis Dorsa in order to (i) measure crater-retention age of fluvial activity using the frequency of superimposed craters; (ii) measure sedimentation rate using the frequency of synfluvial craters (Kite et al. 2013c); (iii) obtain a lower bound on the time gap represented by unconformities, by counting craters

embedded at the unconformity and dividing by estimates of past cratering rates (Werner & Tanaka 2011, Robbins et al. 2013); (iv) if part of the size-frequency distribution of craters has a power-law slope consistent with cratering-erosion steady state (Smith et al. 2008), we will also constrain recent aeolian erosion rates using cratering-erosion balance. The purpose of the chronologic framework is to constrain thickness-to-time conversion factors, and define a ‘floating’ chronology for Aeolis Dorsa. We will additionally attempt (to the extent possible from orbital data) to peg this floating chronology to other deposits on Mars and to absolute time.

2.4.3.2. Paleohydraulic constraints from river deposit measurements. Deliverables (in the form of figures and tables in published manuscripts) will include a longitude-elevation cross-section to highlight trends in each metric with stratigraphic height, logs of parameters versus stratigraphy for each transect, and fence diagrams to correlate transects. Our maps are tailored for a specific science purpose; they are not intended as general-purpose planetary geologic maps. The utility of HiRISE- and CTX-resolution data for measuring paleohydraulic proxies is

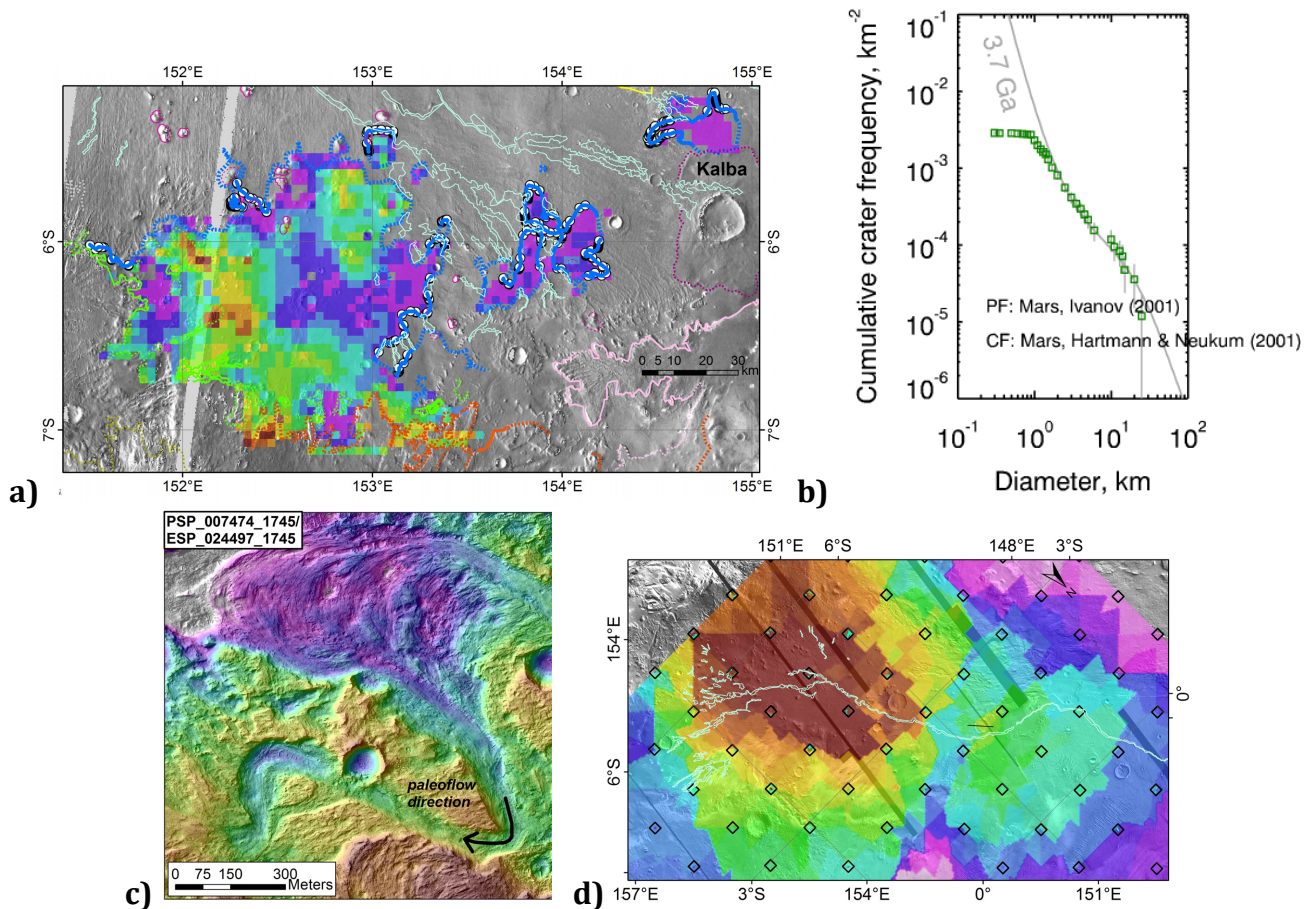


Fig. 5. Preliminary work for Task 2. (a) *Stratigraphic control.* Kriged isopach map of part of unit “F2” (Fig. 2) controlled to MOLA PEDR spots (white circles) located <150 m from “definite” contacts (solid dark blue lines). Purple is thin and red is thick; summed volume is 1061 km³. Proposed work will improve process and extend to all units. (b) *Chronologic control.* Crater count complete to 1.5km plotted using Craterstats2 (Michael & Neukum 2010). Proposed work will count all craters >250m. (c) Part of one of our HiRISE DTMs; chute cutoff (depth 2m) as well as scroll bar truncation are well resolved. Depth of chute cutoff is 2m. (d) Relative channel-deposit density map interpolating between partial mapping (black boxes) of channels. Although widths and wavelengths will be measured only for transects shown in Fig. 2, proposed work will include complete mapping of channel-deposit density.

demonstrated by previous publications (e.g., Burr et al. 2010), as well as our preliminary work.

Metrics: (i) *Paleoflow direction from scroll-bar accretion trajectories and truncation asymmetry.* Flow direction is important for process interpretation (e.g. diBiase et al. 2013) and also constrains paleotilt and sediment transport pathways (Heller et al. 2003). In Aeolis Dorsa, subtle postfluvial deformation (Lefort et al. 2012) renders modern slopes an unreliable guide to paleoflow direction. However, meanders tend to migrate downstream (Lagasse et al., 2004), truncating earlier-deposited scroll bars, which usually accrete on the upstream side of meander bends. In preliminary work, we have mapped meander-truncation vergence directions (Carter 2003) across Aeolis Dorsa ($n = 281$ meanders, of which 271 covered by HiRISE), inferring drainage mainly towards the current trough. This implies paleo-topography was a subdued version of modern topography. We will test, refine and extend this preliminary analysis via a complete repick on stereo companions with significantly different lighting geometry, and calibration using mono images of Martian meanders at Eberswalde, Jezero, and Saheki (where paleoflow direction is known). We will then look for trends of flow direction with stratigraphy.

(ii) *Paleodischarge estimation from channel widths.* We will obtain estimates of paleodischarge using terrestrial width-discharge scalings (e.g. Irwin et al. 2008). The approach for this metric is similar to Burr et al. 2010. We will go beyond this by stratigraphic logging to yield mean and maximum paleodischarge as a function of height, and incorporating into our final estimates resampling error using the underlying terrestrial calibration points for the scalings (e.g. Williams 1988).

(iii) *Paleodischarge from meander wavelengths.* We will parameterize meanders (Howard & Hemberger 1991) by taking the centerlines of each individual meandering channel in the transects and transforming them to $\{L, \varphi\}$ coordinates, where L is distance along the channel, and φ is azimuth relative to meander-belt centerline. (We will separately measure the meander-belt centerlines by taking the centerline of the concave hull of each meander belt.) We will then plot $\partial\varphi/\partial L$ as a function of L . Meander half-wavelength is the Cartesian distance between inflections (zero-crossings of $\partial\varphi/\partial L$). We will manually measure in more complex settings. Discharge-wavelength scalings are an independent crosscheck on width-derived paleodischarge (Irwin et al. 2008, Irwin 2011).

(iv) *Paleoflow direction from meander asymmetry.* Inertia displaces stream thalwegs (and maximum erosive potential) downstream of the bend, so meander bends evolve into a convex-downstream/concave-upstream shape (Kinoshita meanders; Parker & Andrews 1986), with only rare exceptions (Seminara et al., 2001). In a convex-downstream/concave-upstream system, extrema in $\partial\varphi/\partial L$ precede zero-crossings of $\partial\varphi/\partial L$ moving upstream, defining the meander asymmetry and thus likely paleoflow direction. This provides an independent measure of paleoflow direction, especially useful where scroll bars are not preserved.

(v) *Log local sinuosity and 'relative' sinuosity.* We will constrain drainage-network evolution by measuring sinuosity as a function of stratigraphy. Changes in sinuosity with stratigraphic height may reflect changes in discharge, or limited duration of wet events.

(vi) *Fluvial-deposit volume from channel-deposit density.* Using the catalogue of channel deposits, we will map channel-deposit density across Aeolis Dorsa on a 10km x 10km grid (Fig. 5d). We will convert from channel-deposit area to channel-deposit volume using 2 parallel methods: (i) assuming terrestrial scalings as documented in Gibling (2006); (ii) direct measurement of channel deposit width/thickness ratios in areas with HiRISE DTMs, extrapolated to region. In convergent networks, density constrains distance to headwaters (e.g. Malin et al. 2010), and in avulsing systems, it constrains Net/Gross ratio (N/G). By assuming that the

currently exposed channel-deposit density is a representative sample of the fluvial-deposit volume, we will combine these measurements with isopachs to obtain the basin's total volume and length of fluvial channel deposits.

(vii) *Channel formation mechanism from confluence intersection angles.* We will test the hypothesis that some of the river networks formed from groundwater discharge in unconsolidated sediment (Harrison et al. 2013). We will test this by measuring all junction angles, which average 72° (both in theory and in the field; Devauchelle et al., 2012) under such conditions. This contrasts with the branching angles predicted for integration of interdune drainage (~90° for longitudinal dunes), and for minimum dissipation for which angle varies in a predictable way with discharge/width ratio (Howard 1990, Pieri 1984). If junction angles are inconsistent with the prediction, this would indicate that *either* the channels were not formed in unconsolidated sediment, *or* that the water source was not groundwater.

(viii) *Maximum length of networks as a proxy for climate state.* In a cold and/or arid background climate, larger discharge allows longer rivers (Carr 1983). We will interpolate between channel-deposit outcrops, documenting the distances preserved and the distances interpolated (we will separately log drainage integration without any interpolation). Using drainage integration as a proxy for runoff production requires several assumptions. Most importantly, the initial topography at the start of each wet event is assumed to be smoothly sloping, without many local pits. This is justified by the near-constant channel-deposit orientations observed in our preliminary work. Near-surface hydraulic conductivity is assumed not to change with time (not unreasonable in an aggrading system). Finally, river deposits preferentially record the waning stages of wet intervals, and peak runoff might correspond to fluvial-incision unconformities (which we will document separately). In that case we would predict each unconformity-bound fluvial unit records a measurable drying-upward trend.

(ix) *Oxbow lake sedimentation predictions from nature of cutoffs.* We will document the diversion (opening) angles for all cutoffs, and compare with interpreted cutoff mechanism (chute or neck cutoff). Opening angles regulate sedimentation and thus the potential for preservation of organic matter in oxbow lakes (Constantine et al. 2010), which is higher for floodplain deposits than for aeolian, alluvial-fan, or fluvial-channel deposits (Summons et al. 2011).

(x) *Constrain origin of a candidate regional marker bed.* In addition to geological units at 10² m stratigraphic scale, our preliminary work has identified cut-and-fill sedimentary sequences at 1-10m stratigraphic scale, defined by truncation of channels by subsequent channel generations (Fig. 5c) and by multilevel channel deposits (Burr et al. 2009). Using our DTMs, we will carry out regional correlation of a candidate marker bed – a multilevel channel belt (less sinuous over more sinuous). We will document the regional extent of this marker bed; regional coherence would support allocyclic dynamics. We will then use the regional extent and variability to evaluate multiple working hypotheses for the origin of this multilevel channel belt. These hypotheses include:- autocyclic dynamics, with regional correlation maintained by base-level control; allocyclic dynamics, with draping deposits (ash or distal ejecta) stochastically resetting the system; and allocyclic dynamics with shut down and restart of fluvial deposition on a 1-10m stratigraphic scale, consistent with orbitally-paced runoff on Early Mars.

2.4.3.3. Volumes and timescales and constraints on runoff intensity, intermittency, event number, and event duration. Starting from macrostratigraphy output (§2.4.3.1), we will backstrip the basin to recover the original decompacted sediment volume (Nadon & Issler 1997, Allen & Allen 2005). Using fluvial-deposit volumes and the runoff intensity (paleodischarge) for each fluvial unit (calculated in §2.4.3.2), we will apply existing sediment

transport models to obtain runoff durations (Kite 2012). Specifically, we will use analytic models (reviewed in Kleinhans 2005, Kleinhans 2010), scaled to Mars gravity (similar approach to Burr et al. 2010), as well as simple 1D diffusive models of watershed-scale sediment transport (Armstrong et al. 2011), to obtain minimum flow timescales (Kite 2012). We will separately report results using only channel reaches with <50% agreement between 2 or more independent paleohydraulic proxies (wavelength, width), and results using all channel reaches with a proxy. There is a range of discharge – sediment transport relations in the literature, and we will report the sensitivity of our results to this range as well as to variations in modal grain size (0.2 mm vs. 20 mm) and paleoslope (10^{-5} – 10^{-2}). In addition to extremal sensitivity tests, we will track uncertainty using jackknife resampling and report best-estimates as well as 2σ lower limits on timescale. Intermittency will be estimated by dividing flow timescales by the total sediment-accumulation timescale obtained from embedded-crater frequency (§2.4.3.1; Kite et al. 2013c). Minimum total years with runoff and maximum intermittency define a lower bound on the habitability of the time slice corresponding to each geologic unit.

2.4.4. Task 3. Analysis of alluvial-fan catchments to constrain Early Mars surface energy balance.

In this Task, we will generate CTX DTMs (e.g. Fig. 6) for the source catchments of large, relatively young alluvial fans, in order to measure i) geological traces of valley-network erosional efficiency (valley-network slopes and valley volumes), and ii) catchment geometry and viewsheds. We will then model paleo-insolation for all past orbital conditions using our snowmelt model, ISEE-Mars (Kite et al. 2013a). At least 14 craters satisfy our study criteria, which are:- has network; latitude $>17.5^\circ$ (N or S); lacks ice; and catchments that do not extend beyond crater rim. Using the nomenclature of Kraal et al. (2008), these 14 craters are M/Harris (1), L (3), K/Saheki (5), H/Holden (8), J/Jones (1), P (1), S/Ostrov (1), F (1), E (2), D/Luba (2), C/Gringuaz (3), A/Roddy (3), W (1), and X/Majuro (2). (The numbers in parentheses are the number of CTX stereopairs on the PDS with good coverage of our specific measurement targets.) We will select at least 7 craters for detailed analysis, and construct at least 1 CTX DTM for each of these (HRSC DTMs do not adequately resolve small networks; HiRISE stereo covers only small portions of networks). We will mask out landslide deposits and areas affected by midlatitude glaciation. We will test for structural control by plotting rose diagrams of valley lengths versus local angle relative to crater centers. To each short (~250m) segment in the network of valley floors ($>1 \text{ km}^2$ contributing area), we will use the DTMs to assign the contributing area, the local slope, and a 2D histogram including slope and orientation of all contributing pixels. We will then test for correlations between valley-network erosion efficiency and catchment insolation. We will do this firstly by simple regressions (both within individual craters, and between craters). We will additionally use our model, ISEE-Mars, to compute insolation and predicted melt for every catchment, for every season, for all possible orbital conditions, for a P range from 6-250 mbar, and for a range of parameterizations of snowpack stability (Kite et al. 2013a thoroughly documents the model). We will assume solar luminosity 80% of modern, snow albedo of 0.3, and consider thermal inertias of $2000 \text{ J m}^{-2} \text{ K}^{-1} \text{ s}^{-1/2}$ (ice) and $277 \text{ J m}^{-2} \text{ K}^{-1} \text{ s}^{-1/2}$ (snow).

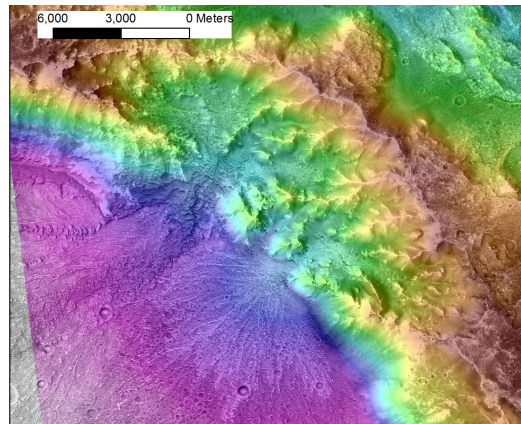


Fig. 6. Portion of CTX DTM (by Collaborator Lucas) resolving valleys sourcing alluvial fans in Harris Crater.

The snowmelt model is not intended to directly invert for absolute values of paleo-environmental parameters. Rather, it is a flexible exploratory tool to establish whether or not seasonal melting under a thin atmosphere predicts the observed sign and *relative* magnitude of aspect dependence. If it does not, that would favor thicker ($\geq 1/4$ bar) atmospheres. We will refine the model from Kite et al. (2013a) by including slope and terrain (viewshed) effects. The relationships between topography and snow accumulation at small scales, and between seasonal snowpack thermal maturation and runoff production, are very complex. We will not attempt to model these processes in detail. Instead, we will assume that *within the source catchments* snow is available during the melt season on all slopes for at least some orbital conditions, and calculate energy-limited runoff production for those conditions. The effects of infiltration and refreezing will be

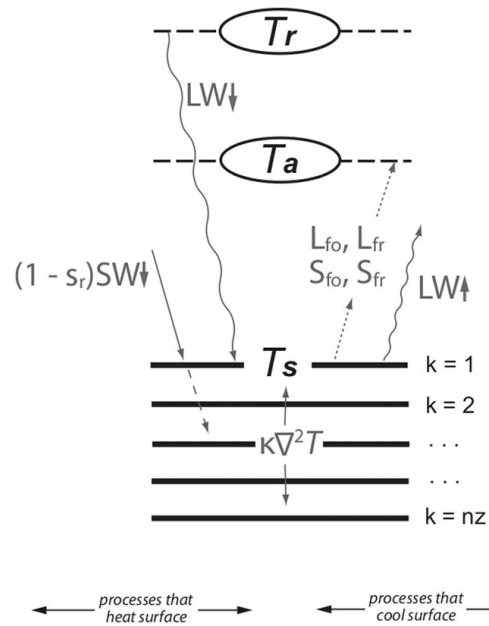


Fig. 7. Vertical discretization and energy flow in ISEE-Mars. Solid horizontal lines: solid surface layers numbered $k = \{1 \dots nz\}$. Dashed horizontal lines: atmospheric layers. T_r is effective atmospheric radiative temperature, T_a is atmospheric surface layer temperature, and T_s is ground surface temperature. Diagonal arrows correspond to energy fluxes: $-LW\downarrow$ = greenhouse effect; $(1 - s_r)SW\downarrow$ = insolation attenuated by Rayleigh scattering; $LW\uparrow$ = back-radiation; $\{L_{fo}, L_{fr}, S_{fo}$ and $S_{fr}\}$ are turbulent fluxes. Solid state greenhouse effect is included. $\kappa\nabla^2 T$ is conductive diffusion. (See Kite et al. 2013a for details).

parameterized by fits to semi-empirical terrestrial models (e.g. Martinec & Rango 1986). Lags between peak runoff and peak discharge are neglected because the catchments are small, and we will assume simple relationships between runoff and sediment transport.

2.5. Perceived Impact of the Proposed Work.

Each climate parameter to be constrained is a fundamental unknown about the Early Mars climate system. The parameters to be constrained are also complementary. As one example, certain impact-rainfall scenarios (Segura et al. 2008) can produce rainfall in thin atmospheres, but not for long periods. Therefore an impact-induced climate change model for ancient runoff on Mars might satisfy the paleopressure constraint and also the timescale constraint, but not the combination of these two constraints.

Aeolis Dorsa is comparable in size, thickness and age to Meridiani, but has been much less studied. Our work may enable global correlation (Edgett 2005). We hypothesize that Aeolis Dorsa is a reference section for global environmental change on Mars.

In addition to the core implications for runoff and climate emphasized in §2.3 and §2.4, paleopressure is a key constraint on ancient aeolian processes, very important in the Martian rock record (Grotzinger & Milliken 2012, Kite et al. 2013b). Task 2 will probe the hypothesis that an ocean once filled the Northern Plains of Mars (Clifford & Parker 2001, di Achille & Hynek 2010), because large river systems respond rapidly to sea-level change (Shen et al. 2012) leaving distinctive patterns of clinoforms (Cateneuneu 2006), detectable through analysis of our isopachs.

2.6. Relevance of the Proposed Work.

The proposed work addresses high-priority Investigations described in the most recent MEPAG report (MEPAG 2010/2012), most directly II.C.2 (“Find physical and

chemical records of past climates”). Based on published correlations between Aeolis Dorsa and Aeolis Mons (Zimbelman & Scheidt 2012), Task 2 may help define the global environmental context for MSL’s fieldwork at Gale. Task 2 characterizes habitability and organic-matter preservation potential at a candidate 2020 landing site (Appendix 6 in Mustard et al., 2013). Task 1 is highly complementary, and Task 3 is also complementary, to a primary objective of the MAVEN mission, “Constraining the Total Atmospheric Loss Through Time” (Jakosky 2013), as well as MSL SAM $\delta^{13}\text{C}$ measurements (Mahaffy et al. 2013).

2.7 Plan of Work

	ACTIVITIES (Task 1 in blue. Task 2 in red. Task 3 in green.)
Year 1	Construct additional DTMs for all Tasks. Train graduate student on ArcGIS and SOCET SET. Begin measuring embedded crater size-frequency distributions. Refine cratering model. Deliverable: LPSC presentation. Refine stratigraphic and chronologic framework for Aeolis Dorsa. Begin measurements of river-deposit dimensions relative to stratigraphic framework. Deliverable: LPSC presentation. Begin measurements of young valley network slopes.
Year 2	Continue construction of additional DTMs for all Tasks. Carry out data-model comparisons. Quantify paleopressure. Deliverable: Detailed manuscript on paleopressure constraints. (Task 1 complete). Continue measuring river-deposit dimensions relative to stratigraphic framework. Deliverable: Short GRL-length manuscript summarizing paleohydrologic constraints for at least 1 transect. Begin computing look-up table of runs of the forward snowmelt model. Continue measurements of young valley network slopes.
Year 3	Basin-wide correlations. Calculate volumes and timescales. Deliverable: Detailed manuscript interpreting paleohydrologic trends with space and relative time across Aeolis Dorsa. Calculate metrics and interpret in terms of snowmelt model. Deliverable: Short GRL-length manuscript interpreting orientation dependences.

2.8 Personnel, Qualifications, and Data-Sharing Plan.

PI **Edwin Kite** is currently a Caltech postdoc and a research associate at the University of Chicago (UChicago); he will be an Assistant Professor at UChicago from 1 Jan 2015. As PI, he will participate to some degree in all aspects of the proposed work and oversee its implementation. Co-I **Jean-Pierre Williams** (UCLA) will carry out a major part of Task 1, specifically implementation and refinement of the forward model of crater-atmosphere interactions. Collaborator **Alan Howard** (U. Virginia) will assist for all Tasks in interpretation of the GIS in terms of erosional and depositional processes. Collaborator **Antoine Lucas** (Université Paris 7) will assist in interpretation and quality control of existing DTMs, and inter-lab DTM quality crosschecks. A **graduate student** at UChicago will carry out much of the stratigraphic work, and assist in constructing DTMs. The graduate student will play little or no role in Task 1, but a major role in Tasks 2 and 3. All personnel will participate in interpretation of results. A **planetary GIS/data specialist** at UChicago will support GIS and data integration for all tasks, and will assist in DTM production; no funds are requested for this specialist, who will be supported by UChicago through Kite’s startup funds. All DTMs will be publicly released immediately after production, at climatefutures.com/stereo. All GIS files will be publicly mirrored at midnight on the 1st of each month at climatefutures.com/data. We will discuss with the PDS and USGS the possibility of mirroring end products at PDS/PIGWAD. (FTE information is contained in the Budget Justification).

3. References and citations.

- Allen, P.A., & Allen, J.R. (2005), Basin analysis: principles and applications (2nd edition), Blackwell.
- Amundson, R. et al. (2012), Geomorphologic evidence for the late Pliocene onset of hyperaridity in the Atacama Desert, *Geological Society of America Bulletin*, 124(7-8), 1048-1070.
- Armitage, J.J. et al. (2011), Timescales of alluvial fan development on Mars. *Geophys. Res. Lett.*, 38, CiteID L17203.
- Baker, V.R., et al. (1991), Ancient oceans, ice sheets and the hydrological cycle on Mars, *Nature*, 352, 589-594.
- Balme, M., et al. (2006), Orientation and distribution of recent gullies in the southern hemisphere of Mars: Observations from High Resolution Stereo Camera/Mars Express (HRSC/MEX) and Mars Orbiter Camera/Mars Global Surveyor (MOC/MGS) data, *J. Geophys. Res.*, 111, E5, CiteID E05001.
- Beitler, B., et al. (2003), Bleaching of Jurassic Navajo Sandstone on Colorado Plateau Laramide Highs: Evidence of Exhumed Hydrocarbon Supergiants?, *Geology*, 31(12), 1041-1044.
- Brown P., et al. (2002), The flux of small near-Earth objects colliding with the Earth. *Nature* 420, 294–296.
- Buczowski, Debra L. et al. (2005), Buried impact craters: A topographic analysis of quasi-circular depressions, Utopia Basin, Mars, *Journal of Geophysical Research*, 110, E3, CiteID E03007.
- Burr, Devon M.; Enga, Marie-Therese; Williams, Rebecca M. E.; Zimelman, James R.; Howard, Alan D.; Brennand, Tracy A. (2009), Pervasive aqueous paleoflow features in the Aeolis/Zephyria Plana region, Mars, *Icarus*, 200, 52-76.
- Burr, Devon M.; Williams, Rebecca M. E.; Wendell, Kimberly D.; Chojnacki, Matthew; Emery, Joshua P. (2010), Inverted fluvial features in the Aeolis/Zephyria Plana region, Mars: Formation mechanism and initial paleodischarge estimates, *Journal of Geophysical Research*, 115, CiteID E07011.
- Carr, M. H. (1983), Stability of streams and lakes on Mars, *Icarus*, 56, 476 – 495.
- Carter, D.C. (2003), 3-D seismic geomorphology: Insights into fluvial reservoir deposition and performance, Widuri field, Java Sea, *AAPG Bulletin*, 87(6), 909–934.
- Catling, D.C. (2009), Atmospheric evolution of Mars. p. 66-75 in: V. Gornitz (ed.) *Encyclopedia of paleoclimatology and ancient environments*, Springer, Dordrecht.
- Catuneanu, O. (2006), *Principles of Sequence Stratigraphy*, Elsevier Science.
- Cepilecha, Z., et al. (1998) Meteor phenomena and bodies, *Space Sci. Rev.*, 84, 327-341.
- Clifford, S.M., & Parker, T.J. (2001), The Evolution of the Martian Hydrosphere: Implications for the Fate of a Primordial Ocean and the Current State of the Northern Plains, *Icarus*, 154(1), 40-79.
- Clow, G. D. (1987), Generation of liquid water on Mars through the melting of a dusty snowpack, *Icarus* 72, 95-127.
- Constantine, J.A., et al. (2010), Controls on the alluviation of oxbow lakes by bed-material load along the Sacramento River, California, *Sedimentology*, 57, 389-407.
- Conway, S.J. & Mangold, N. (2013), Evidence for Amazonian mid-latitude glaciation on Mars from impact crater asymmetry, *Icarus*, 225, 413-423.
- Costard, F., et al. (2002), Formation of Recent Martian Debris Flows by Melting of Near-Surface Ground Ice at High Obliquity, *Science*, 295, 110-113.

- Daubar, I.J., et al. (2013), The current martian cratering rate, *Icarus* 225, 506-516.
- Davila, A.F., et al. (2013), Evidence for Hesperian glaciation along the Martian dichotomy boundary, *Geology*, 41(7), 755-758.
- Davis, P. (1993), Meteoroid impacts as seismic sources on Mars, *Icarus*, 105, 469-478.
- Devauchelle, O., et al. (2012), Ramification of stream networks, *Proc. National Acad. Sci.*, 109, 20832-20836.
- di Achille, G. & Hynek, B.M. (2010), Ancient ocean on Mars supported by global distribution of deltas and valleys, *Nature Geoscience*, 3, 459-463.
- diBiase, R.A., et al. (2013), Deltaic deposits at Aeolis Dorsa: Sedimentary evidence for a standing body of water on the northern plains of Mars, *J. Geophys. Res.- Planets*, 118, 1285-1302.
- Dickson, J.L.; Head, J.W.; & Kreslavsky, M., (2007), Martian gullies in the southern mid-latitudes of Mars: Evidence for climate-controlled formation of young fluvial features based upon local and global topography, *Icarus*, 188, 315-323.
- Donsellar, M.E., & Overeem, I., (2008), Connectivity of fluvial point-bar deposits: an example from the Miocene Huesca fluvial fan, Ebro Basin, Spain, *AAPG Bulletin* 92(9), 1109-1129.
- Edgett, K.S. (2005), The sedimentary rocks of Sinus Meridiani: Five key observations from data acquired by the Mars Global Surveyor and Mars Odyssey orbiters, *International Journal of Mars Science and Exploration*, 1, 5-58.
- Egholm, D.L., et al. (2009), Glacial effects limiting mountain height, *Nature*, 460, 884-887.
- Ehlmann, B.L. et al. (2011), Subsurface water and clay mineral formation during the early history of Mars. *Nature* 479, 53–60.
- Fassett, C.I., and Head, J.W. (2008), The timing of martian valley network activity: Constraints from buffered crater counting, *Icarus*, 195, 1, 61-89.
- Foreman, B.Z., et al. (2012), Fluvial response to abrupt global warming at the Palaeocene/Eocene boundary. *Nature*, 491, 92-95.
- Forget, F., et al. (2013), 3D modeling of the early martian climate under a denser CO₂ atmosphere: Temperatures and CO₂ ice clouds, *Icarus*, 222, 81-99.
- Forsberg-Taylor, N.K., Howard, A.D., & Craddock, R.A. (2004), Crater degradation in the Martian highlands: Morphometric analysis of the Sinus Sabaeus region and simulation modeling suggest fluvial process, *J. Geophys. Res.* 109, E05002.
- Gibling, M. R. (2006), Width and Thickness of Fluvial Channel Bodies and Valley Fills in the Geological Record: A Literature Compilation and Classification, *Journal of Sedimentary Research*, 76, 731-770.
- Grant, J.A. & Wilson, S.A. (2011), Late alluvial fan formation in southern Margaritifer Terra, Mars, *Geophys. Res. Lett.*, 38, 8, CiteID L08201.
- Grant, J., & Wilson, S.A. (2012), A possible synoptic source of water for alluvial fan formation in southern Margaritifer Terra, Mars. *Planet. & Space Sci.*, 72, 1, 44-52.
- Grotzinger, J.P., Milliken, R.E., 2012. The sedimentary rock record of Mars: Distribution, origins, and global stratigraphy. In: Grotzinger, J.P. (Ed.), *Sedimentary Geology of Mars*, Special Publications, vol. 102. SEPM (Society for Sedimentary Geology), 1–48
- Haberle, R. M.; et al. (2012), A Cloud Greenhouse Effect on Mars: Significant Climate Change in the Recent Past? 43rd Lunar and Planet. Sci. Conf., The Woodlands, Texas. LPI Contribution No. 1659, id.1665

- Hackney, C. & Carling, P. (2011), The occurrence of obtuse junction angles and changes in channel width below tributaries along the Mekong River, south-east Asia, *Earth Surface Processes and Landforms*, 36(12), 1563–1576.
- Hajek, E.A., & Wolinsky, M.A. (2012), Simplified process modeling of river avulsion and alluvial architecture: Connecting models and field data, *Sedimentary Geology*, 257-260, 1-30.
- Harrison, S. K.; Balme, M. R.; Hagermann, A.; Murray, J. B.; Muller, J.-P.; Wilson, A. (2013), A branching, positive relief network in the middle member of the Medusae Fossae Formation, equatorial Mars—Evidence for sapping? *Planet. & Space. Sci.*, 85, 142-163.
- Hauber, E.; van Gasselt, S.; Chapman, M. G.; Neukum, G. (2008), Geomorphic evidence for former lobate debris aprons at low latitudes on Mars: Indicators of the Martian paleoclimate, *J. Geophys. Res.*, 113, E2, CiteID E02007.
- Heller, P.L., & Paola, C. (1996), Downstream changes in alluvial architecture: an exploration of controls on channel-stacking patterns, *Journal of Sedimentary Research*, 66(2), 297-306.
- Heller, P.L., Dueker, K., and McMillan, M.E. (2003), Post-Paleozoic alluvial gravel transport as evidence of continental tilting in the U.S. Cordillera, *Geological Society of America Bulletin*, 115, 1122-1132.
- Hoke, M.R.T.; Hynek, B.M.; Tucker, G.E. (2011), Formation timescales of large Martian valley networks, *Earth and Planetary Science Letters*, 312, 1, 1-12.
- Holsapple, K.A. (1993), The scaling of impact processes in planetary sciences, *Ann. Rev. Earth Planet. Sci.* 21, 333-373.
- Howard, Alan D. (1990), Theoretical Model of Optimal Drainage Networks, *Water Resources Research*, 26(9), 2107-2117.
- Howard, Alan D., & Allen T. Hemberger (1991), Multivariate characterization of meandering, *Geomorphology*, 4, 161-186.
- Howard, A.D. (2007), Simulating the development of Martian highland landscapes through the interaction of impact cratering, fluvial erosion, and variable hydrologic forcing, *Geomorphology* 91, 332-363.
- Howard, A. D. (2009), How to make a meandering river, *Proceedings of the National Academy of Sciences*, 106, 17245-17246.
- Howard, Alan D.; Moore, Jeffrey M.; Irwin, Rossman P. (2005), An intense terminal epoch of widespread fluvial activity on early Mars: 1. Valley network incision and associated deposits, *J. Geophys. Res.*, 110, E12, CiteID E12S14.
- Hynek, B., & di Achille, G. (in press), *Geologic Map of Meridiani Planum & Correlation of Mapped Units*, U.S. Geological Survey Astrogeology Program.
- Irwin, Rossman P., III; Craddock, Robert A.; Howard, Alan D. (2005), Interior channels in Martian valley networks: Discharge and runoff production, *Geology*, 33(6), 489-
- Irwin, R. P., Howard, A. D., Craddock, R. A. (2008), Fluvial valley networks on Mars, in Roy et al., eds, *River Confluences, Tributaries, and the Fluvial Network*, Wiley, p. 419-450.
- Irwin, R. P. (2011), Timing, Duration, and Hydrology of the Eberswalde Crater Paleolake, Mars, 42nd Lunar and Planetary Science Conference, LPI Contribution No. 1608, p.2748
- Jakosky, B., (2013), The 2013 MAVEN mission to Mars (August 2013 update).
http://lasp.colorado.edu/home/maven/files/2013/09/MAVEN_083013.pdf
- Jerolmack, Douglas J.; Mohrig, David; Zuber, Maria T.; Byrne, Shane (2004), A minimum time for the formation of Holden Northeast fan, Mars, *Geophys. Res. Lett.*, 31, 21, CiteID L21701.

- Kite, E.S. (2012), Evidence for Melt-Fed Meandering Rivers in the Gale-Aeolis-Zephyria Region, Mars Kite, E. S. 43rd Lunar and Planetary Science Conference, held March 19-23, 2012 at The Woodlands, Texas. LPI Contribution No. 1659, id.2778
- Kite, E.S., Halevy, I., Kahre, M.A., Manga, M., & Wolff, M., (2013a), Seasonal melting and the formation of sedimentary rocks on Mars, *Icarus*, 223, 181-210.
- Kite, E.S., Lewis, K.W., Lamb, M.P., Newman, C.E., & Richardson, M.I., (2013b), Growth and form of the mound in Gale Crater, Mars: Slope-wind enhanced erosion and transport, *Geology*, 41, 543-546.
- Kite, E.S., Lucas, A., & C.I. Fassett (2013c), Pacing Early Mars river activity: Embedded craters in the Aeolis Dorsa region imply river activity spanned $\geq(1-20)$ Myr, *Icarus*, 225, 850-855.
- Kite, E.S., Williams, J.-P., Lucas, A., & Aharonson, O. (2013d), Paleopressure of Mars' atmosphere from small ancient craters, accepted in principle by Nature Geoscience, preprint available at arxiv.org/abs/1304.403 (astro-ph:EP).
- Kite, E.S. et al. (2013e), Resolving The Great Drying of Mars: Sequence Stratigraphy of The Aeolis-Zephyria Trough, DPS-AAS Annual Meeting, Denver, CO, DPS meeting #45, abstract #405.07.
- Kirk, R.L., et al. (2008), Ultrahigh resolution topographic mapping of Mars with MRO HiRISE stereo images: Meter-scale slopes of candidate Phoenix landing sites, *J. Geophys. Res.* 113, E00A24.
- Kleinhans, M.G. (2005). Flow discharge and sediment transport models for estimating a minimum timescale of hydrological activity and channel and delta formation on Mars, *J. Geophys. Res.*, 110, E12003.
- Kleinhans, M.G., H.E. van de Kastele and E. Hauber (2010), Palaeoflow reconstruction from fan delta morphology on Mars, *Earth and Planetary Science Letters*, 294, 378-392.
- Kraal, E.R., et al. (2008), Catalogue of large alluvial fans in martian impact craters, *Icarus*, 194, 1, 101-110.
- Kreslavsky, M. A.; Head, J. W. (2003) North-south topographic slope asymmetry on Mars: Evidence for insolation-related erosion at high obliquity, *Geophys. Res. Lett.*, 30, CiteID 1815.
- Lagasse, P.F., et al. (2004), Handbook for predicting stream meander migration, Part 1, National Cooperative Highway Research Program, National Research Council (U.S.) Transportation Research Board.
- Lammer, H., et al. (2013), Outgassing history and escape of the Martian atmosphere and water inventory, *Space Sci. Rev.* 174, 113-154
- Lefort, A., et al. (2012), Inverted fluvial features in the Aeolis-Zephyria Plana, western Medusae Fossae Formation, Mars: Evidence for post-formation modification, *J. Geophys. Res.*, 117, E3, CiteID E03007.
- Loizeau, D., et al. (2012), Chronology of deposition and alteration in the Mawrth Vallis region, Mars, *Planetary and Space Science*, 72, 31-43.
- Levy, J.S., et al. (2013), Garwood Valley, Antarctica: A new record of Last Glacial Maximum to Holocene glaciofluvial processes in the McMurdo Dry Valleys, *GSA Bulletin*, 125, 1484-1502.
- Macdonald, F.A., et al. (2012), Early Neoproterozoic basin formation in the Yukon, *Geoscience Canada*, 39, 77-99.
- Macklin, M.G., et al. (2012), The fluvial record of climate change, *Philos. Trans. A Math Phys. Eng. Sci.*, 370(1966), 2143-72.

- Mahaffy, P.R., et al. (2013), Abundance and isotopic composition of gases in the martian atmosphere from the Curiosity rover, *Science* 341, 263-266.
- Malin, M.C., et al., (2010), An overview of the 1985-2006 Mars Orbiter Camera science investigation, *International Journal of Mars Science and Exploration*, 4, 1-60
- Manga, M.; Patel, A.; Dufek, J., Kite, E.S. (2012), Wet surface and dense atmosphere on early Mars suggested by the bomb sag at Home Plate, Mars, *Geophys. Res. Lett.*, 39, 1, CiteID L01202.
- Mangold, N., et al. (2004), Evidence for Precipitation on Mars from Dendritic Valleys in the Valles Marineris Area, *Science*, 305, 78-81.
- Mangold, N., et al. (2012), A chronology of early Mars climatic evolution from impact crater degradation, *J. Geophys. Res.*, 117, CiteID E04003
- Manning, C.V., McKay, C.P., and Zahnle, K.J. (2006), Thick and thin models of the evolution of carbon dioxide on Mars, *Icarus*, 180, 38-59.
- Martinec, J., & Rango, A. (1986), Parameter values for snowmelt runoff modeling, *J. Hydrology*, 84, 197-219.
- McNamara, J.P., & Kane, D.L., 2008, The impact of a shrinking cryosphere on the form of arctic alluvial channels, *Hydrologic Processes* 23, 159-168.
- MEPAG (2010/2012), Mars Scientific Goals, Objectives, Investigations, and Priorities: J.R. Johnson, ed., (2012 version for review), posted by the Mars Exploration Program Analysis Group, (MEPAG) at <http://mepag.jpl.nasa.gov/reports/index.html>.
- Miall, A.D., 2002, Architecture and sequence stratigraphy of Pleistocene fluvial systems in the Malay Basin, based on seismic time-slice analysis, *American Association of Petroleum Geologists Bulletin*, 86(7), 1201-1216.
- Michael G.G., Neukum G., (2010), Planetary surface dating from crater size-frequency distribution measurements: Partial resurfacing events and statistical age uncertainty, *Earth and Planetary Science Letters*, 294, 223-229.
- Milliken, R. E.; et al. (2010), Paleoclimate of Mars as captured by the stratigraphic record in Gale Crater, *Geophys. Res. Lett.*, 37, 4, CiteID L04201.
- Mischna, M.A., et al. (2013), Effects of obliquity and water vapor/trace gas greenhouses in the early martian climate, *J. Geophys. Res. Planets*, 118, 560-576.
- Moore, J.M., & Howard, A.D. (2005), Large alluvial fans on Mars, *J. Geophys. Res.*, 110, E4, CiteID E04005.
- Morgan, G.A., et al. (2010), Gully formation on Mars: Two recent phases of formation suggested by links between morphology, slope orientation and insolation history, *Icarus*, 208, 658-666.
- Morgan, A.M., Howard, A.D., Hobley, D.E.J., Moore, J.M., Dietrich, W.E., Williams, R.M.E., Burr, D.M., Grant, J.A., Wilson, S.A., and Matsubara, Y. (in press), Sedimentology and climatic environment of alluvial fans in the Martian Saheki Crater and a comparison with terrestrial fans in the Atacama Desert, *Icarus*.
- Mustard, J., et al. (2013), Report of the Mars 2020 Science Definition Team (Appendix 6: Candidate Landing Site Supporting Information), downloaded from <http://mars.jpl.nasa.gov/mars2020/>
- Nadon, G.C. & Issler, D.R. (1997), The compaction of floodplain sediments: Timing, magnitude and implications, *Geoscience Canada* 24(1), 37-43.
- Noe Dobrea, E. Z.; Bishop, J. L.; McKeown, N. K.; Fu, R.; Rossi, C. M.; Michalski, J. R.; Heinlein, C.; Hanus, V.; Poulet, F.; Mustard, R. J. F.; Murchie, S.; McEwen, A. S.; Swayze, G.; Bibring, J.-P.; Malaret, E.; Hash, C. (2010), Mineralogy and stratigraphy of

- phyllosilicate-bearing and dark mantling units in the greater Mawrth Vallis/west Arabia Terra area: Constraints on geological origin, *Journal of Geophysical Research*, Volume 115, Issue E11, CiteID E00D19.
- Parker, G. & Andrews E.D. (1986), On the time development of meander bends, *Journal of Fluid Mechanics*, 162, 139-156.
- Parsons, R. A. et al. (2013), Evidence for a short period of hydrologic activity in Newton crater, Mars, near the Hesperian-Amazonian transition, *J. Geophys. Res.- Planets*, 118, 1082-1093.
- Penido, Julita C.; Fassett, Caleb I.; Som, Sanjoy M. (2013), Scaling relationships and concavity of small valley networks on Mars, *Planet. & Space. Sci.*, 75, 105-116.
- Petroff, A.P., et al., (2012), Four remarks on the growth of channel networks, *Comptes Rendus Geoscience*, 344, 33-40.
- Pieri, D.C., (1984), Junction Angles in Drainage Networks, *J. Geophys. Res.* 89(B8), 6878-6884.
- Pollack, J.B., Kasting, J.F., Richardson, S.M., & Poliakoff, K. (1987), The case for a wet, warm climate on early Mars, *Icarus* 71, 203-224.
- Rasmussen, C.E., and Williams, C.K.I., (2006), *Gaussian Processes for Machine Learning*, MIT Press, 2006. ISBN 0-262-18253-X.
- Reijnenstein, Hernan M. et al. (2011), Seismic geomorphology and high-resolution seismic stratigraphy of inner-shelf fluvial, estuarine, deltaic, and marine sequences, Gulf of Thailand, *AAPG Bulletin*, 95, 1959-1990.
- Robbins, Stuart J.; Hynek, Brian M.; Lillis, Robert J.; Bottke, William F. (2013), Large impact crater histories of Mars: The effect of different model crater age techniques, *Icarus*, 225, 1, 173-184.
- Scanlon, K.E., et al. (2013), Orographic precipitation in valley network headwaters: Constraints on the ancient Martian atmosphere, *Geophys. Res. Lett.* 40, 1–6.
- Segura, Teresa L., Toon, O. Brian, and Colaprete, Anthony (2008), Modeling the environmental effects of moderate-sized impacts on Mars, *J. Geophys. Res. – Planets* 113, E11007.
- Segura, Teresa L.; McKay, Christopher P.; Toon, Owen B. (2012), An impact-induced, stable, runaway climate on Mars, *Icarus*, 220, 144-148.
- Seminara, G., et al. (2001), Downstream and upstream influence in river meandering. Part 2. Planimetric development. *Journal of Fluid Mechanics* 438, 213-230.
- Shanley, K.W., & McCabe, P.J., 1994, Perspectives on the sequence stratigraphy of continental strata, *American Association of Petroleum Geologists Bulletin* 78(4), 544-568.
- Shen Z., et al. (2012), Rapid and widespread response of the Lower Mississippi River to eustatic forcing during the last glacial-interglacial cycle: *Geological Society of America Bulletin*, 124, 690–704.
- Sloss, L.L. (1963), Sequences in the cratonic interior of North America, *Geol. Soc. Am. Bulletin*, 74(2), 93-
- Smith, Matthew R., et al. (2008), Effect of obliteration on crater-count chronologies for Martian surfaces, *Geophys. Res. Lett.*, 35, 10, CiteID L10202.
- Stanley, B.D., et al. (2012), CO₂ solubility in primitive martian basalts similar to Yamato 980459, the effect of composition on CO₂ solubility of basalts, and the evolution of the martian atmosphere, *American Mineralogist*, 97, 1841-1848.
- Straub, K.M., et al. (2009), Compensational stacking of channelized sedimentary deposits, *Journal of Sedimentary Research*, 79, 673–688.
- Summons, Roger E.; Amend, Jan P.; Bish, David; Buick, Roger; Cody, George D.; Des Marais, David J.; Dromart, Gilles; Eigenbrode, Jennifer L.; Knoll, Andrew H.; Sumner, Dawn Y.

- (2011), Preservation of Martian Organic and Environmental Records: Final Report of the Mars Biosignature Working Group, *Astrobiology*, 11, 157-181.
- Toon, Owen B.; Segura, Teresa; Zahnle, Kevin (2010), The Formation of Martian River Valleys by Impacts, *Annual Review of Earth and Planetary Sciences*, 38, 303-322.
- Turcotte, D.L., et al., (1981), Role of membrane stresses in the support of planetary topography, *J. Geophys. Res.*, 86, 3951-3959.
- Urata, R.A., & Toon, O.B., (2013) Simulations of the martian hydrologic cycle with a general circulation model: Implications for the ancient martian climate, *Icarus*, 226, 229-250.
- Vasavada, A.R., Milavec, T.J., and Paige, D.A., (1993), Microcraters on Mars: Evidence for Past Climate Variations, *J. Geophys. Res.* 98, 3469-3476.
- Wall, J.V. & Jenkins, C.R., (2012), *Practical statistics for astronomers*, 2nd Edition (Cambridge Observing Handbooks for Research Astronomers), Cambridge University Press, Cambridge, UK.
- Wang, Y., et al. (2011), Scale-dependent compensational stacking: An estimate of autogenic time scales in channelized sedimentary deposits, *Geology*, 39, 811-814.
- Ward, P. D., Montgomery, D. R. & Smith, R. (2000), Altered river morphology in South Africa related to the Permian–Triassic extinction, *Science*, 289, 1740–1743.
- Werner, S. C.; Tanaka, K. L. (2011), Redefinition of the crater-density and absolute-age boundaries for the chronostratigraphic system of Mars, *Icarus*, 215, 603-607.
- Williams, G. P. (1988), Paleofluvial estimates from dimensions of former channels and meanders, in *Flood Geomorphology*, edited by V. R. Baker et al. pp. 321–334, Wiley, New York.
- Williams, J.-P., Pathare, A.V., and Aharonson, O. (2013), The production of small primary craters on Mars and the Moon. Arxiv:astro-ph:EP , <http://arxiv.org/abs/1309.2849>.
- Williams, R.M.E., et al., (2011), Evidence for episodic alluvial fan formation in far western Terra Tyrrhena, Mars, *Icarus*, 211, 222-237.
- Williams, R.M.E., et al. (2013), Variability in martian sinuous ridge form: Case study of Aeolis Serpens in the Aeolis Dorsa, Mars, and insight from the Mirackina paleoriver, South Australia, *Icarus*, 225, 308-324.
- Wilson, S. A., et al. (2013), Inventory of Equatorial Alluvial Fans and Deltas on Mars, 44th Lunar and Planetary Science Conference, The Woodlands, Texas. LPI Contribution No. 1719, p.2710
- Wordsworth, R., et al. (2010), Infrared collision-induced and far-line absorption in dense CO₂ atmospheres, *Icarus*, 210, 992-997.
- Wordsworth, R., et al. (2013), Global modelling of the early martian climate under a denser CO₂ atmosphere: Water cycle and ice evolution, *Icarus*, 222, 1, 1-19.
- Zimbelman, J.R., & Scheidt, S.P. (2012), Hesperian age for Western Medusae Fossae Formation, Mars, *Science*, 336, 1683.

4. Biographical Sketches.

Edwin S. Kite (Principal Investigator).

Professional preparation:

B.A. Cambridge University (Natural Sciences Tripos – Geological Sciences), June 2007
M.Sci. Cambridge University (Natural Sciences Tripos – Geological Sciences), June 2007
Ph.D. University of California Berkeley (Earth and Planetary Science), December 2011

Appointments:

Assistant Professor, Department of the Geophysical Sciences, University of Chicago
from January 2015
(*research associate with PI status from August 2013*)

Harry Hess Fellow (50% Astrophysical Sciences, 50% Geoscience), Princeton University
from January 2014 – December 2014

O.K. Earl Fellow, Geological and Planetary Sciences Division, Caltech
January 2012 – January 2014.

Papers from the past 15 months:

Kite, E.S., Williams, J.-P., Lucas, A., & Aharonson, O., “Paleopressure of Mars' atmosphere from small ancient craters,” accepted by *Nature Geoscience*, preprint available at arxiv.org/abs/1304.403 (astro-ph:EP)

Kite, E.S., Lewis, K.W., Lamb, M.P., Newman, C.E., & Richardson, M.I., 2013, “Growth and form of the mound in Gale Crater, Mars: Slope-wind enhanced erosion and transport,” *Geology*, 41, 543-546. (“Highlight of the Meeting” at Science).

Kite, E.S., Halevy, I., Kahre, M.A., Manga, M., & Wolff, M., 2013, “Seasonal melting and the formation of sedimentary rocks on Mars,” *Icarus*, 223, 181-210.

Kite, E.S., Lucas, A., & C.I. Fassett, “Pacing Early Mars river activity: Embedded craters in the Aeolis Dorsa region imply river activity spanned $\approx(1-20)$ Myr,” *Icarus*, 225, 850-855.

Mangold, N., **Kite, E.S.**, Kleinhans, M., Newsom, H.E., Ansan, V., Hauber, E., Kraal, E., Quantin-Nataf, C. & K. Tanaka, 2012, “The origin and timing of fluvial activity at Eberswalde Crater, Mars,” *Icarus*, 220, 530-551.

Šrámek, O., McDonough, W., **Kite, E.S.**, Lekic, V., Zhong, S.T., & Dye, W.F., Geophysical and geochemical constraints on geoneutrino fluxes from Earth's mantle, *Earth Planet. Sci. Lett.*, doi:10.1016/j.epsl.2012.11.001. (“Research Highlight” at Nature).

Rappaport, S., Levine, A., Chiang, E., El Mellah, I., Jenkin, J., Kalomeni, B., **Kite, E.S.**, Kotson, M., Nelson, L., Rousseau-Nepton, & Tran, K., 2012, “Possible disintegrating short-period Super-Mercury orbiting KIC 12557548,” *Astrophys. J.*, 752, 1.

(Page 1 of 2)

Additional papers on Mars or planetary habitability:

Kite, E.S., Michaels, T.I., Rafkin, S.C.R., Manga, M., & W.E. Dietrich, 2011. "Localized precipitation and runoff on Mars," *J. Geophys. Res. Planets*, 116, E07002, 20 pp.
doi:10.1029/2010JE003783.

Kite, E.S., Rafkin, S.C.R., Michaels, T.I., Dietrich, W.E., & Manga, M., 2011. "Chaos terrain, storms, and past climate on Mars," *J. Geophys. Res. Planets*, 116, E10002, 26 pp.,
doi:10.1029/2010JE003792 ("Research Highlight" at Nature Geoscience).

Kite, E.S., Gaidos, E. & M. Manga, 2011. "Climate instability on tidally locked exoplanets,"
Astrophys. J., 743, 41, 12 pp.

Manga, M., Patel, A., Dufek, J., & **Kite, E.S.**, 2012. "Wet surface and dense atmosphere on early Mars inferred from the bomb sag at Home Plate, Mars," *Geophys. Res. Lett.*,
doi:10.1029/2011GL050192.

Kite, E.S., Manga, M., & Gaidos, E., 2009. "Geodynamics and rate of volcanism on massive Earth-like planets," *Astrophys. J.*, 700, 1732-1749.

Chiang, E., **Kite, E.**, Kalas, P., Graham, J. R., & Clampin, M., 2009. "Fomalhaut's Debris Disk and Planet: Inferring the Mass and Orbit of Fomalhaut b Using Disk Morphology," *Astrophys. J.*, 693, 734-749.

Kite, E.S., Matsuyama, I., Manga, M., Perron, J.T., & Mitrovica, J.X., 2009, "True polar wander driven by late-stage volcanism and the distribution of paleopolar deposits on Mars,"
Earth Planet. Sci. Lett., 280, 254-267.

Kalas, P., Graham, J. R., Chiang, E., Fitzgerald, M. P., Clampin, M., **Kite, E. S.**, Stapelfeldt, K., Marois, C., & Krist, J., 2008. "Optical Images of a Planet 25 Light Years from Earth," *Science*, 322, 1345-1348 ("Breakthrough of the Year #2" at Science; AAAS Newcomb Cleveland Prize).

Kite, E.S., & R.C.A. Hindmarsh, 2007. "Did ice streams shape the largest channels on Mars?,"
Geophys. Res. Lett., 34, L19202.

Telescope experience:

Hubble Space Telescope: Co-I on GO/DD Program 11818 (PI: Paul Kalas).

Spitzer Space Telescope: Warm IRAC phase curves of exoplanet HAT-P-7b (PI: Heather Knutson).

Field geology experience:

Central India (Proterozoic paleobiology). Greece, SE Spain, England, Scotland, California, Hawaii (fieldwork, mapping courses). NW Spain (independent mapping project, 6 weeks). Utah (GSI for Professor W. Alvarez).

(Page 2 of 2)